ACS APPLIED MATERIALS & INTERFACES

Research Article

Cite This: ACS Appl. Mater. Interfaces 2017, 9, 36103-36110

www.acsami.org

Near-Infrared to Visible Organic Upconversion Devices Based on Organic Light-Emitting Field Effect Transistors

Dongwei Li,[†,‡] Yongsheng Hu,[*,†] Nan Zhang,[†] Ying Lv,[†] Jie Lin,[†] Xiaoyang Guo,[†] Yi Fan,[†] Jinsong Luo,[†] and Xingyuan Liu[*,†]

[†]State Key Laboratory of Luminescence and Applications, Changchun Institute of Optics, Fine Mechanics and Physics, Chinese Academy of Sciences, Changchun 130033, China

[‡]University of Chinese Academy of Sciences, Beijing 100049, China

Supporting Information

ABSTRACT: The near-infrared (NIR) to visible upconversion devices have attracted great attention because of their potential applications in the fields of night vision, medical imaging, and military security. Herein, a novel all-organic upconversion device architecture has been first proposed and developed by incorporating a NIR absorption layer between the carrier transport layer and the emission layer in heterostructured organic light-emitting field effect transistors (OLEFETs). The as-prepared devices show a typical photon-to-photon upconversion efficiency as high as 7% (maximum of 28.7% under low incident NIR power intensity) and millisecond-scale response time, which are the highest upconversion efficiency and one of the fastest response time among organic upconversion devices as referred to the previous reports up to now. The high upconversion performance mainly originates from the gain mechanism of field-effect transistor structures and the unique advantage of OLEFETs to balance between the photodetection and light emission. Meanwhile, the strategy of OLEFETs also offers the advantage of high integration so that no extra OLED is needed in the organic upconversion devices. The results would pave way for low-cost, flexible and portable organic upconversion devices with high efficiency and simplified processing.

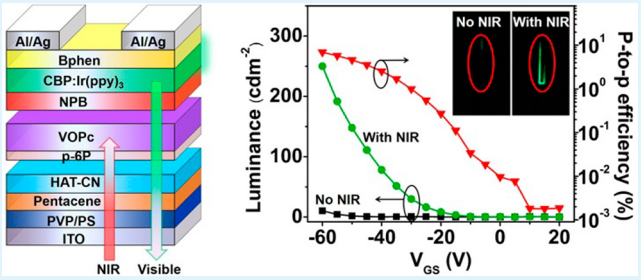

KEYWORDS: *near-infrared to visible, upconversion, organic field-effect transistors, light-emitting, phototransistors*

1. INTRODUCTION

The near-infrared (NIR) to visible upconversion devices have attracted great attention due to their promising applications in the fields of night vision, medical imaging and military security.[1−3] A prevalent approach to accomplish upconversion devices is to integrate an organic/inorganic photodetector (PD) and an organic light-emitting diode (OLED).[4,5] Thereinto, all-organic upconversion devices can offer fascinating functions for low cost, large area, and flexibility in comparison to hybrid structures.[1,6] However, despite the great advances in the device performance, it is not inevitable to obtain a high upconversion efficiency by connecting the PD and OLED in series. One reason is that the internal electric field of the PD and OLED can not be tuned separately in the two terminal upconversion devices, resulting in a performance trade-off between the two parts.[7] Besides, there is an upper limit of 100% for the photon-to-electron (p-to-e) efficiency for common PDs due to the absence of gain mechanism.[8]

For better performance (photon-to-photon (p-to-p) efficiency) of upconversion devices (decided by the product of the p-to-e efficiency of the PD and the electron-to-photon (e-to-p) efficiency of the OLED), an effective approach is to utilize a phototransistor (PT) instead of a PD because PTs can simultaneously achieve light detection and signal amplification (gain) without increasing noise, and thus can obtain much higher p-to-e efficiency than common PDs.[8,9] For instance, by combining with OLEDs, both the p-n-p InGaAs/InP PT and the PbS quantum dot vertical PT have exhibited excellent upconversion efficiency.[7,10,11] Up to now, organic PTs (OPTs) have not been incorporated in upconversion devices, resulting in a very limited p-to-p efficiency for organic upconversion devices.[1,12]

Organic light-emitting field effect transistors (OLEFETs) are a kind of multifunctional optoelectronic devices that integrate both the switching function of organic field-effect transistors (OFETs) and the luminescence function of OLEDs.[13,14] OLEFETs show promising applications in the fields of flat panel displays, sensors, and optical communication,[15−18] and may also become a kind of OPT with high gain because of their basic structure of OFETs. However, to the best of our knowledge, the light detection as well as the upconversion function of the OLEFETs has not yet been explored.

Received: July 19, 2017
Accepted: September 29, 2017
Published: September 29, 2017

DOI: 10.1021/acsami.7b10538
ACS Appl. Mater. Interfaces 2017, 9, 36103−36110

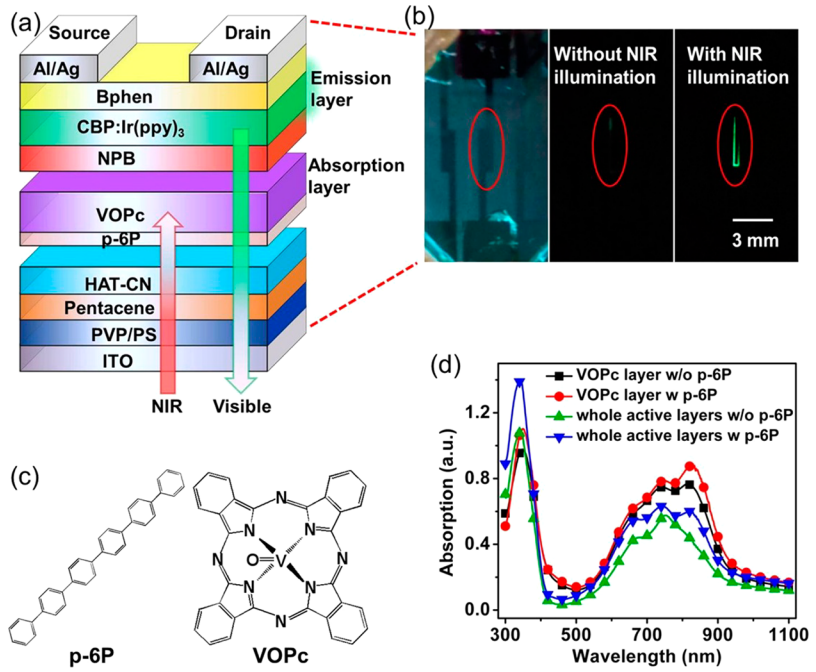

Figure 1. (a) Schematic of the upconversion devices based on OLEFETs. (b) Optical images of a working device with (right) and without (middle) the NIR illumination. The unconverted green emission is visible in the right image. The left is the image of a device without bias voltage under bright background. (c) Molecular structures of p-6P and VOPc. (d) Absorption spectra of the VOPc film (60 nm) and the whole active layers (including the dielectric layer) with and without p-6P on quartz substrates.

In this work, on the basis of OLEFETs, we propose a novel device architecture for the NIR to visible organic upconversion devices, showing a typical p-to-p efficiency as high as 7%, a maximum value of 28.7% when under low incident NIR light intensity, and millisecond-scale response time. It is revealed that the high performance originates mainly from the gain mechanism of OLEFETs and their unique advantage to balance between the photodetection and light emission. Meanwhile, there is no need to make extra OLEDs owing to the high integration of OLEFETs, which offers potential opportunity to simplify the structure of high-efficiency NIR to visible upconversion devices.

2. EXPERIMENTAL SECTION

The schematic of the devices is shown in Figure 1a. The devices can be fabricated by simply evaporating a NIR absorption layer between the carrier transport layer and the emission layer in common heterostructured OLEFETs. Vanadyl-phthalocyanine (VOPc, molecular structure in Figure 1c) is used as the NIR absorption layer, before which an inducing layer of para-sexiphenyl (p-6P, molecular structure in Figure 1c) is used. The other layers constitute the typical OLEFETs, among which, the indium tin oxide (ITO) works as the gate electrode, 400 nm poly-4-vinylpenol (PVP)/30 nm polystyrene (PS) acts as the dielectric layer (capacitance $C_i \sim 7.5$ nFcm^{-2}), pentacene (12 nm), 1,4,5,8,9,11-hexaazatriphenylene hexacarbonitrile (HAT-CN, 2 nm)/N,N′-di(naphthalene-1-yl)-N,N′-diphenyl-benzidine (NPB, 10 nm), 4,4′-bis(carbazol-9-yl)biphenyl:Fac-tris(2-phenylpyridinato) iridium-(III) (CBP:Ir(ppy)$_3$, 25 nm, 6 wt %), and bathophenanthroline (Bphen, 14 nm) act as the hole transport layer, hole injection layer, emission layer, and electron injection layer and are successively evaporated at the rates of 0.15, 0.05, 0.15, 0.05, 1.6, and 0.2 Å/s, respectively. The source/drain electrodes are constituted by a thin Al (1 nm) and Ag (100 nm) with channel length and width of 45 and 3000 μm, respectively. The devices were encapsulated in the glovebox (H_2O, O_2< 0.1 ppm) before test. The light emission from the device was collected from the ITO side, whereas the NIR incident light illuminated from the ITO side for the upconversion measurement.

The electrical characteristics were performed by Keithley 4200 SCS at room temperature under ambient air. The photocurrent was recorded by HAMAMATSU S1336 photodiode. The NIR incident light for upconversion measurement is a diode laser (continuous wave) with the wavelength of 808 nm. The incident light intensity was carefully calibrated by THORLABS PM320E optical power and energy meter. The wavelength dependence characteristic was measured by utilizing a lock-in amplifier at a chopping frequency of 120 Hz under illumination by monochromatic light from a xenon lamp. The response characteristic was measured by combining the diode laser with a Tektronix DPO5104 digital phosphor oscilloscope. The crystal structure of VOPc films were analyzed by X-ray diffraction (XRD, D8-DISCOVER, Bruker). The atomic force microscopy (AFM) measurement was performed on a Shimadzu SPM-9700. The absorption spectra were measured by UV-3101PC UV−vis-NIR spectrophotometer and the electroluminescence (EL) spectra of the devices were measured by AvaSpec-ULS2048L fiber spectrometer. The carrier mobilities were calculated by the formula for the saturation regime: $I_{DS} = \mu C_i(W/2L)(V_{GS} - V_{Th})^2$ (where μ is the field-effect mobility, C_i is the gate dielectric capacitance density, V_{Th} is the threshold voltage, W and L are the channel width and length, respectively). The brightness was calculated by comparing the photocurrent with a standard OLED of known brightness (1000 cdm^{-2}) and emission area (3 mm × 1 mm) with structure of ITO/NPB/CBP:Ir(ppy)$_3$/Bphen/LiF/Al. The EQE was calculated from the brightness, the drain current and electroluminescent (EL) emission spectrum assuming Lambertian emission.

3. RESULTS AND DISCUSSION

As a widely adopted organic photosensitive material, VOPc can exhibit three paramorphs involving amorphous phase, monoclinic crystal structure (phase I) and triclinic crystal structure (phase II), which can be generally distinguished by their absorption spectra.[19,20] The absorption spectrum of B band for the amorphous phase and monoclinic crystal structure (molecular axis perpendicular to the substrate) is around 330−360 nm, while the absorption spectrum of Q-band is around 710−760 nm. The triclinic crystal structure (molecular

DOI: 10.1021/acsami.7b10538
ACS Appl. Mater. Interfaces 2017, 9, 36103−36110

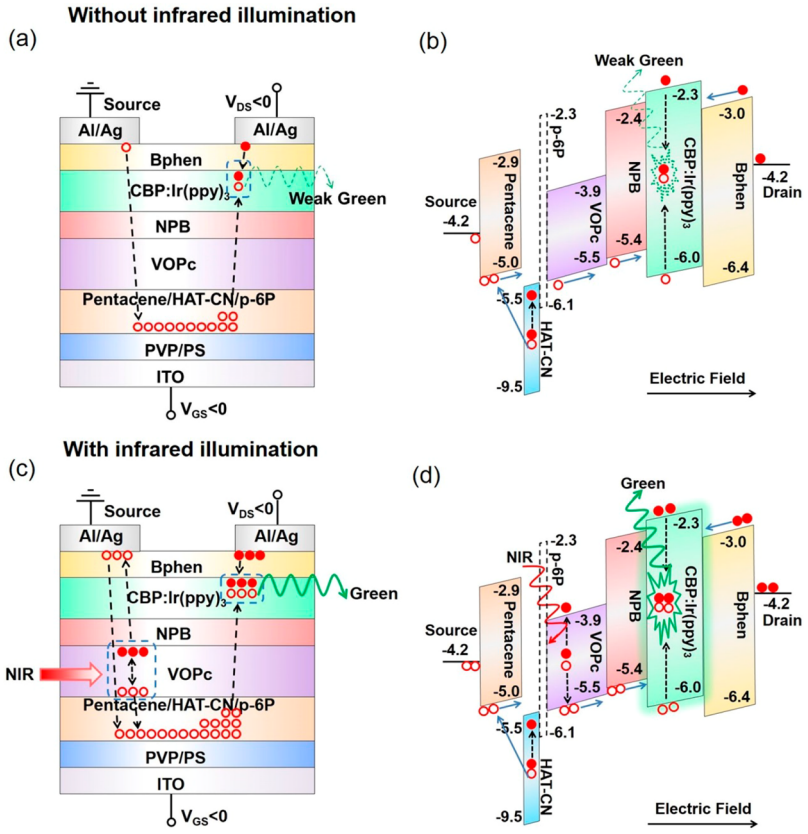

Figure 2. Schematic representations of (a) carrier injection and transport, and (b) the corresponding working mechanism without NIR illumination. Schematic representations of (c) carrier injection and transport, and (d) the corresponding working mechanism with NIR illumination. Note that the ultrathin layer of p-6P is shown by a dashed box in b and d because of its negligible hole blocking effect as described in the text. In b and d, the charge generation and transfer process from HAT-CN to pentacene mainly happen under the source electrode because of the applied bias voltage.

axis parallel to the substrate) shows similar absorption spectrum of B band to the monoclinic crystal structure, but a red-shifted absorption spectrum of Q-band around 810−850 nm. Therefore, to enhance the NIR absorption of the devices, triclinic crystal structure of VOPc is more desired. For this purpose, we introduced an ultrathin p-6P (~3 nm) as the inducing layer,[21] which has been used to epitaxially induce highly oriented VOPc film with triclinic crystal structure by choosing an appropriate substrate and controlling the growth condition to change the arrangements of molecules in grown film.[22] The absorption spectra of the VOPc films with and without p-6P inducing layer on a quartz substrate are shown in Figure 1d. Both films show similar absorption peak of Q-band at 742 nm, however, there is a stronger absorption peak at 830 nm for the VOPc film induced by p-6P layer, indicating the existence of more triclinic crystal arrangements for the VOPc film induced by p-6P. Similar results can be found from the absorption spectra for samples with the whole organic active layers: the absorption peak for samples without p-6P is at 752 nm, while a new absorption peak emerges at 825 nm for the p-6P induced samples. It illustrates that the use of ultrathin p-6P inducing layer is a facile and efficient method for preparing VOPc films with triclinic crystal structure.

The influence of the p-6P inducing layer on the growth of VOPc film can be further understood by the XRD patterns (Figure S1a). For VOPc film evaporated on pentacene/HAT-CN substrate without p-6P, there are two distinct diffraction peaks at $2\theta = 7.5°$ and $2\theta = 26.3°$, which correspond to phase II and phase I,[20,23] respectively. For VOPc film with p-6P inducing layer, the diffraction peak at $2\theta = 26.3°$ disappears, which indicates that the VOPc film is mainly in phase II. Likewise, a stronger diffraction peak at $2\theta = 7.5°$ is observed for VOPc film with p-6P evaporated directly on quartz substrate compared to that without p-6P. These results are in consistent with those from the absorption spectra. Figure S1b shows the AFM morphology of different organic films. The roughness of VOPc film with p-6P increases slightly compared to that without p-6P, which probably arises from the higher roughness of p-6P (surface roughness: R_q = 5.3 nm) than HAT-CN (R_q = 4.1 nm). The VOPc film with p-6P also shows larger average grain size (~75 nm) than that without p-6P (~60 nm), which is in accordance with the XRD patterns which have a better crystallinity of phase II for the samples with p-6P inducing layer. The better crystallinity of phase II means a stronger absorption in NIR region,[20,24] which also agrees with the absorption spectra. Figure S1c presents the absorption spectra for other organic active layers, which shows negligible absorption in the NIR region.

Figure 2 describes the working mechanism for the NIR upconversion devices. Because of the hole-dominated characteristic of pentacene, the devices are generally biased under gate to source voltage (V_{GS}) < 0 V and drain to source voltage (V_{DS}) < 0 V to ensure the hole accumulation mode. In this mode, when there is no NIR illumination, as described in Figure 2a, b, the holes will be injected from the source electrode and accumulate to form a conducting channel at the interface between pentacene and the dielectric layers. Near the bottom of the drain electrode, the accumulated holes in the channel will

DOI: 10.1021/acsami.7b10538
ACS Appl. Mater. Interfaces 2017, 9, 36103−36110

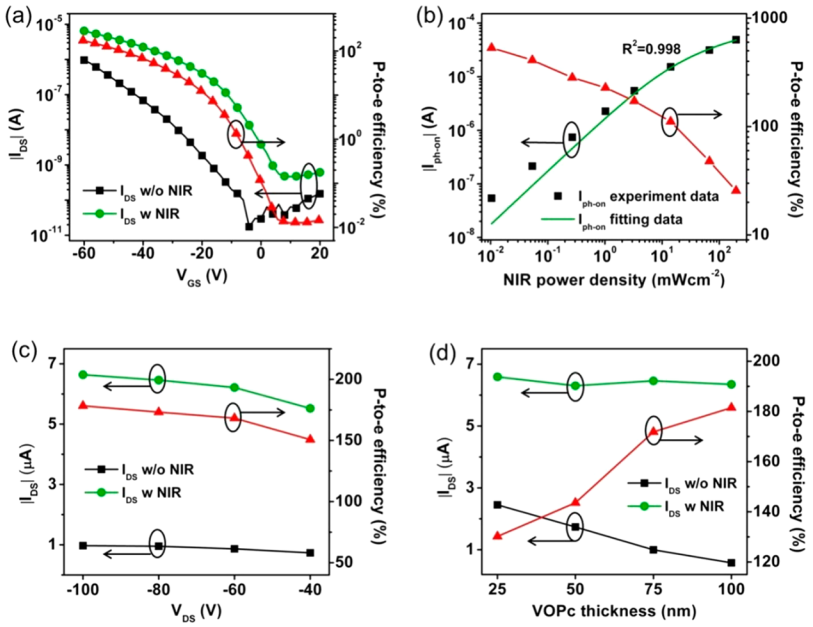

Figure 3. (a) Transfer curves of the devices with and without the illumination at V_{DS} = −80 V, and the corresponding p-to-e efficiency. (b) Measured and fitted results of the photocurrent at different incident light intensities and the corresponding p-to-e efficiency at V_{GS}=-60 V, V_{DS} = −80 V. (c) Drain current of the devices with and without the illumination at different V_{DS} with fixed V_{GS} = −60 V, and the corresponding p-to-e efficiency. (d) Drain current of the devices with and without the illumination for VOPc thickness of 25, 50, 75, and 100 nm at V_{GS} = −60 V, V_{DS} = −80 V, and the corresponding p-to-e efficiency.

move toward the emission layer under the vertical electric field and form excitons with the electrons injected from the drain electrode. It is noticed that the HOMO level of VOPc (−5.5 eV)[25] is very close to that of NPB (−5.4 eV),[26] therefore the incorporation of VOPc probably will not bring large hole injection barrier. Although the HOMO level of p-6P is relatively high (−6.1 eV),[27] we presume that it do not cause serious influence on the transport of holes since the thickness is only one molecular layer. Actually, the drain current for p-6P induced devices is much higher than that for noninduced ones, as is shown in Figure S2. The increase of the drain current presumably originates from the change of the crystal structure of VOPc since phase II is more conducive for the carrier transport than phase I[28] due to large intermolecular π-orbit overlap and short intermolecular distance of the highly π-stacked structure for phase II.[29] The interfacial layer of HAT-CN can significantly promote the concentration of holes by charge transfer with the p-type materials which we have discussed in a previous study.[30]

When under NIR illumination, considering the absorption property of the used organic active layers (Figure S1c), the incident light will be mainly absorbed by the VOPc layer where excitons are generated (Figure 2c and 2d). The photogenerated excitons can be separated into electrons and holes efficiently near the source electrode due to the vertical electric field. The electrons will move across NPB/CBP:Ir(ppy)$_3$ and Bphen and finally accumulate under the source electrode, where they can effectively lower the hole injection barrier, resulting in an effective decrease of the contact resistance and a concomitantly positive shifted threshold voltage.[31,32] The photogenerated holes, together with the injected holes from the source electrode, will move down to pentacene and accumulate in the channel, followed by transporting along the interface of dielectric/pentacene because of the horizontal electric field. Finally, the accumulated holes will transport into the emission layer followed by exciton formation with the electrons injected from the drain electrode.

Because the upconversion efficiency (p-to-p) depends on the characteristics of both the photodetection (p-to-e) and light emission (e-to-p) of the devices, we will discuss each of them respectively in the following. To minimize the errors, for each kind of structures in the work, we analyzed at least 6 samples for average.

Figure 3 presents the photodetection characteristics of the devices. In the transfer curves (Figure 3a, V_{DS} = −80 V), there is a distinct increase of the drain current for devices under NIR illumination (3.26 mW cm^{-2}) compared to that in dark (transfer curves for different incident light intensities are shown in Figure S3a). Meanwhile, the threshold voltage shifts positively for more than 20 V, which can be ascribed to the decrease of the contact resistance at the source electrode as described above. The p-to-e efficiency ($EQE_{p-e} = \frac{hc}{q\lambda}R$, where $\frac{hc}{\lambda}$ is the photon energy, q is the electron charge, R is the photoresponsivity, $R = \frac{I_{light} - I_{dark}}{P_{inc}}$, I_{light} is the drain current under NIR illumination, I_{dark} is the drain current in dark, and P_{inc} is the incident NIR power on the channel area) increases as the gate voltage (V_{GS}) increases negatively because the photo-generated carriers separate more easily under higher vertical electric field. The p-to-e efficiency reaches 173.2%, which is greater than 100%, at V_{GS} = −60 V, demonstrating gain machanism in the OLEFETs when they function as OPTs.

To better understand the role of OPTs for the OLEFETs, we further look into the operation mechanisms of the devices. Generally, two kinds of effects can happen in OPTs when under illumination. For $V_{GS} < V_{Th}$, the p-type OPTs are biased under the on-state, and the drain current is mainly affected by the photovoltaic effect. In this case, the photocurrent ($I_{ph.pv}$) can be expressed as[9,33]

DOI: 10.1021/acsami.7b10538
ACS Appl. Mater. Interfaces 2017, 9, 36103−36110

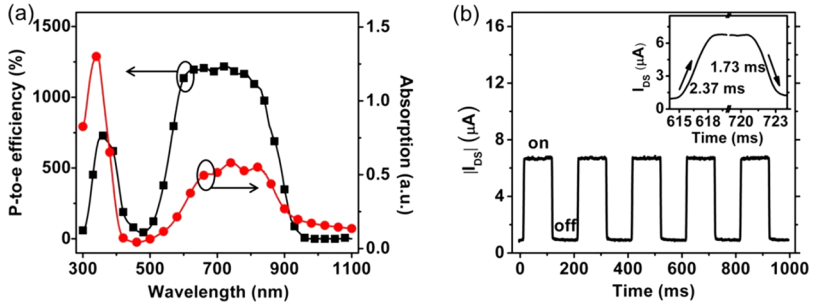

Figure 4. (a) Absorption of the whole active layers and the wavelength dependence of the p-to-e efficiency of the devices under ~2.5 μW cm^{-2} at V_{GS} = −60 V, V_{DS} = −80 V. (b) Response characteristic of the devices under 3.2 mW cm^{-2} at V_{GS} = −60 V, V_{DS} = −80 V. The inset shows one of the periods.

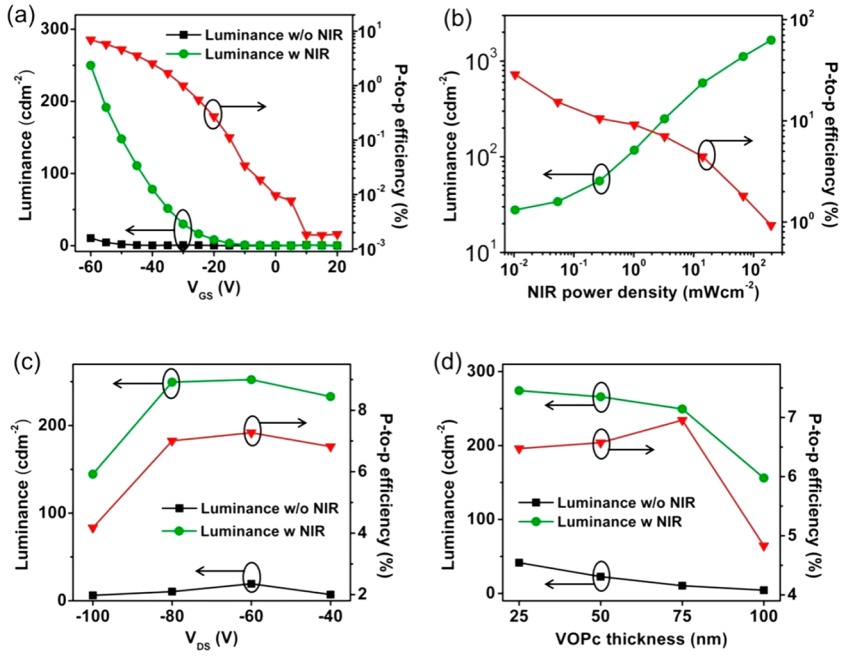

Figure 5. Upconversion light emission characteristics of the devices. (a) Transfer curves of brightness with and without the NIR illumination (3.26 mW cm^{-2}) and the corresponding p-to-p efficiency at V_{DS} = −80 V. (b) Brightness and the corresponding p-to-p efficiency under different incident light intensities at V_{GS} = −60 V, V_{DS} = −80 V. (c) Brightness with and without the NIR illumination (3.26 mW cm^{-2}) for different V_{DS} and the corresponding p-to-p efficiency at V_{GS} = −60 V. (d) Brightness with and without the NIR illumination (3.26 mW cm^{-2}) for different thickness of VOPc and the corresponding p-to-p efficiency at V_{GS} = −60 V, V_{DS} = −80 V.

$$I_{ph.pv} = g_m \Delta V_{Th} = \frac{AkT}{q} \ln\left(1 + \frac{\eta q \lambda P_{inc}}{I_{dark} hc}\right) \quad (1)$$

where $g_m = dI_{DS}/dV_{GS}$ represents the transconductance of the devices, A is a proportionality parameter, k is the Boltzmann constant, T is the operating temperature, λ is the wavelength of the incident light, η is the external quantum efficiency, h denotes Planck's constant, and P_{inc} is the incident NIR power. Figure 3b shows the relationship between the photocurrent ($I_{ph\text{-}on}$) and the incident light intensity of the devices under the on-state (V_{GS} = −60 V, V_{DS} = −80 V). Both the $I_{ph\text{-}on}$ and the threshold voltage shift (Figure S3b) can be well-fitted by eq 1 (coefficient of determination are 0.998 and 0.985, respectively), which indicates that the devices follow the photovoltaic effect when working under the on-state. On the other hand, when $V_{GS} > V_{Th}$, the p-type OPTs are biased under the off-state. The drain current will change with the incident light intensity because of the photoconductive effect, in this case, the photocurrent follows by[9]

$$I_{ph.pc} = (q\mu_p pE)WD = BP_{inc} \quad (2)$$

herein, μ_p represents the hole mobility, p is the hole concentration, $E = V_{DS}/L$ is the lateral electric field in the channel, W is the gate width, D is the absorption depth of the active layer, and B is the fitting parameter. Similarly, the photocurrent of the devices under the off-state can be well fitted by eq 2 (coefficient of determination R^2 = 0.983), indicating that the devices follow the photoconductive effect under the off-state.

Figure 3b also shows the p-to-e efficiency at different incident light intensities. When the incident light is weak (~10.4 μW cm^{-2}), the p-to-e efficiency can be higher than 530%. It decreases gradually with the increasing of the incident light power density, which agrees well with most OPT-only devices, and can be mainly ascribed to the recombination of the photogenerated carriers.[34] Figure 3c shows the drain current at different V_{DS} (V_{GS} = −60 V) and the corresponding p-to-e efficiency. As V_{DS} increases negatively, the I_{light} improves gradually, whereas the I_{dark} keeps relatively stable, accordingly,

DOI: 10.1021/acsami.7b10538
ACS Appl. Mater. Interfaces 2017, 9, 36103−36110

Table 1. Summary of the Primary Characteristics of the Upconversion Devices in This Work

devices VOPc (nm)	p-6P (w or w/o)	mobility (dark) ($cm^2 V^{-1} s^{-1}$)	threshold voltage shift (V)[a]	brightness (w/o NIR) ($cd m^{-2}$)	brightness (w NIR) ($cd m^{-2}$)[a]	p-to-e efficiency (%)[a]	p-to-p efficiency (%)[a]
25	w	0.058 ± 0.05	13.5 ± 1.6	41.5 ± 3	274 ± 20	130.2 ± 10	6.47 ± 0.5
50	w	0.038 ± 0.05	19.7 ± 2	22.6 ± 1	266 ± 20	143.6 ± 10	6.57 ± 0.5
50	w/o	0.023 ± 0.03	18.7 ± 2	5.96 ± 1	44 ± 5	49.5 ± 6	0.67 ± 0.1
75	w	0.022 ± 0.04	21.7 ± 2	10.4 ± 1	250 ± 15	171.9 ± 11	7.0 ± 0.4
100	w	0.013 ± 0.03	28.1 ± 2.4	4.3 ± 0.5	156 ± 13	181.5 ± 12	4.83 ± 0.4

[a]The values are obtained under illumination of 3.26 mW cm^{-2} at V_{GS} = −60 V, V_{DS} = −80 V.

the p-to-e efficiency increases. It is also noticed that for V_{DS} higher than −60 V, the change gradually flattens, which indicates that most of the photogenerated carriers have been separated.[35,36] The detailed output curves for devices with and without the illumination are shown in Figure S3c.

To illustrate the role of the NIR absorption layer in the performance of the devices, Figure 3d presents the p-to-e efficiency of the devices with different thickness of VOPc (25, 50, 75, and 100 nm). When there is no incident light, the drain current decreases gradually as the thickness of VOPc grows. This is reasonable, as the bulk resistance of the active layers will increase because of the relatively poor conductivity of the organic materials. When under illumination, the drain current no longer decreases with the increase of the VOPc due to the existence of photogenerated carriers. Consequently, the p-to-e efficiency improves from 130.1% for 25 nm VOPc to 181.5% for 100 nm VOPc. The influence of the p-6P inducing layer is also evaluated, as is shown in Figure S 3d (50 nm VOPc, 2.08 mW cm^{-2}). The introduce of p-6P brings 2−14 times enhancement for the p-to-e efficiency, which can be attributed to the improved NIR absorption and carrier transport ability[28] for the phase II crystal of VOPc.

We also investigated the wavelength dependence of the devices, as is shown in Figure 4a. The incident light intensity is limited to ∼2.5 μW cm^{-2} by the measurement system. The wavelength dependence is in agreement qualitatively with the absorption spectrum of the device, which shows two high response regions corresponding to the absorption of Q-band and B band for VOPc, respectively. The device maintains a high p-to-e efficiency of more than 765% in the NIR region of 780−860 nm, and the corresponding detectivity ($D^* = \frac{RA^{1/2}}{(2qI_{dark})^{1/2}}$, A is the device area) is higher than 2.08×10^{11} Jones (Figure S4). The response characteristic of the devices is shown in Figure 4b, which is obtained at the incident light intensity of 3.2 mW cm^{-2} and V_{GS} = −60 V, V_{DS} = −80 V. The measurement was performed by utilizing a shutter to switch the incident light on and off with the time duration of 100 ms. The rising (from 10 to 90%) and falling (from 90 to 10%) time of the drain current deduced from the inset of Figure 4b is only 2.37 and 1.73 ms, respectively, indicating a relatively high cutoff frequency (>250 Hz) among the high gain OPTs.[37−39]

The upconversion light emission characteristics of the devices are shown in Figure 5. The luminance of the devices in dark is very low, which is estimated to be only ∼10 cd m^{-2} even at V_{GS} = −60 V (Figure 5a). However, when under illumination (3.26 mW cm^{-2}), the devices lit (∼2.3 cd m^{-2}) at V_{GS} as low as −10 V and the brightness increases rapidly with the negative increase of V_{GS}, and reaches ∼250 cd m^{-2} at V_{GS} = −60 V. The emission spectrum of the devices (Figure S5a) shows a main peak at 514 nm with a shoulder peak around 549 nm, demonstrating the EL emission comes from the emission layer of CBP:Ir(ppy)$_3$.[40] Photographs of a sample with and without the illumination are shown in Figure 1b.

The upconversion efficiency (p-to-p) of the devices can be obtained by

$$\eta_{con} = \frac{\int \frac{\lambda I_{ph}(\lambda)}{R(\lambda)hc} d\lambda}{\frac{\lambda_{IR} P_{IR}}{hc}} \quad (3)$$

where $I_{ph}(\lambda)$ and $R(\lambda)$ are the photocurrent and photoresponsivity of the photodetector collecting the emitted visible photons, respectively, and λ_{IR} and P_{IR} are the wavelength and the incident NIR power on the channel area, respectively. As is shown in Figure 5a, the p-to-p efficiency increases as the V_{GS} increases negatively, and reaches a maximum value of ∼7% at V_{GS} = −60 V. To the best of our knowledge, this is the best result ever reported for all-organic upconversion devices (Table S1). Figure 5b shows the brightness and the corresponding η_{con} of the devices under different incident light intensities at V_{GS} = −60 V, V_{DS} = −80 V. It is noticed that the η_{con} can reach as high as 28.7% under low incident light intensity (10.4 μW cm^{-2}). The brightness increases with the increase of the incident light intensity and a maximum brightness of more than 1600 cd m^{-2} can be obtained under 196 mW cm^{-2} with a corresponding η_{con} of 0.93%. Influenced by the p-to-e efficiency, the p-to-p efficiency of the devices decreases with the increase of the incident light intensity.

Figure 5c shows the brightness and p-to-p efficiency at different V_{DS}. Distinct from that of the p-to-e efficiency, the p-to-p efficiency and brightness of the devices do not increase persistently as V_{DS} varies from −40 V to −100 V, and a remarkable decrease can be found at V_{DS} = −100 V. It indicates that the decrease of the brightness and p-to-p efficiency at high V_{DS} (< −80 V) should arise from the decrease of the e-to-p efficiency of the devices since the p-to-e efficiency increases with the negative increase of V_{DS}. In fact, the e-to-p efficiency of the devices decreases persistently with the negatively increasing of V_{DS} (Figure S5b), which can be probably attributed to the overbalance of holes and electrons resulting from the increased hole injection.[30]

The influence of the thickness of VOPc on the upconversion light emission characteristics is shown in Figure 5d. As the thickness of VOPc increases from 25 to 100 nm, the brightness of the devices reduces persistently. We speculate that it is resulted from the block of holes for thicker VOPc, which can be inferred from the decreased hole mobility for devices with thicker VOPc (Table 1). The hole blocking effect may also reduce the hole injection efficiency from pentacene to the emission layer, resulting in the decrease of the e-to-p efficiency from 5.51% for devices without VOPc to 2.66% for devices with 100 nm VOPc (Figure S5c). Although the e-to-p efficiency is much lower than the EQE of OLEDs based on CBP:Ir(ppy)$_3$ (15% ∼ 20%),[41] considering the simultaneously obtained high

DOI: 10.1021/acsami.7b10538
ACS Appl. Mater. Interfaces 2017, 9, 36103−36110

p-to-e efficiency, the performance still shows an obvious advantage for the OLEFETs to balance between the photodetection and light emission compared with two terminal devices. On the other hand, with the increase of the thickness of VOPc, the p-to-p efficiency first increases and then decreases. It is worth noting that the p-to-p efficiency varies little in a wide range of thickness (25−75 nm), which also signifies that the OLEFETs offer much flexibility for structure design. The primary characteristics of the upconversion devices in this work are summarized in Table 1.

4. CONCLUSION

To summarize, we have successfully demonstrated a class of all-organic NIR to visible upconversion devices based on the OLEFETs. The current gain originated from the basic structure of OFETs ensures a high p-to-e efficiency. Meanwhile, the incorporation of the infrared photosensitive layer does not cause a severe impact on the e-to-p efficiency, guarantying state-of-the-art p-to-p efficiency for the organic upconversion devices. The devices also show good response characteristic. It is believed that by further implementing approaches[14,42,43] such as reducing the channel length, using transport materials with higher carrier mobilities, increasing the gate capacitance, and adopting asymmetric electrodes, there is still much room to improve the comprehensive performance involving the operational voltage, luminance, e-to-p efficiency, and p-to-p efficiency of the devices. The results in this work will not only extend the functionalities of the OLEFETs but also provide some helpful insights for developing flexible and portable NIR to visible organic upconversion devices with high efficiency and simple processes.

■ ASSOCIATED CONTENT

Supporting Information

The Supporting Information is available free of charge on the ACS Publications website at DOI: 10.1021/acsami.7b10538.

XRD patterns, AFM images and absorption spectra of films; transfer curves for devices with and without p-6P inducing layer; transfer curves, off-state photocurrent, and threshold voltage shift of devices under different NIR power densities; output curves of devices with and without NIR; p-to-e efficiency of devices with and without p-6P inducing layer; photodetectivity, EL spectra, and E-to-p efficiency of devices; performance comparison among NIR upconversion devices (PDF)

■ AUTHOR INFORMATION

Corresponding Authors

*E-mail: huyongsheng@ciomp.ac.cn.
*E-mail: liuxy@ciomp.ac.cn.

ORCID

Yongsheng Hu: 0000-0002-8116-4378
Ying Lv: 0000-0003-1649-5258
Xiaoyang Guo: 0000-0003-0259-137X
Xingyuan Liu: 0000-0002-9681-1646

Notes

The authors declare no competing financial interest.

■ ACKNOWLEDGMENTS

This work was supported by the CAS Innovation Program, the National Natural Science Foundation of China (61775211, 51503196, 61405195), the Jilin Province Science and Technology Research Projects (20160520176JH, 20160520092JH, 20150101039JC), and State Key Laboratory of Luminescence and Applications.

■ REFERENCES

(1) Liu, S.; Lee, C.; Yuan, C.; Su, W.; Lin, S.; Chang, W.; Huang, B.; Lin, C.; Lee, Y.; Su, T.; Chen, K. Transparent Organic Upconversion Devices for Near-Infrared Sensing. *Adv. Mater.* **2015**, *27*, 1217−1222.

(2) Chen, J.; Tao, J.; Ban, D.; Helander, M. G.; Wang, Z.; Qiu, J.; Lu, Z. Hybrid Organic/Inorganic Optical Up-Converter for Pixel-Less Near-Infrared Imaging. *Adv. Mater.* **2012**, *24*, 3138−3142.

(3) Chu, X.; Guan, M.; Niu, L.; Zeng, Y.; Li, Y.; Zhang, Y.; Zhu, Z.; Wang, B. Fast Responsive and Highly Efficient Optical Upconverter Based on Phosphorescent OLED. *ACS Appl. Mater. Interfaces* **2014**, *6*, 19011−19016.

(4) Ban, D.; Han, S.; Lu, Z. H.; Oogarah, T.; SpringThorpe, A. J.; Liu, H. C. Near-Infrared to Visible Light Optical Upconversion by Direct Tandem Integration of Organic Light-Emitting Diode and Inorganic Photodetector. *Appl. Phys. Lett.* **2007**, *90*, 093108.

(5) Lv, W.; Zhong, J.; Peng, Y.; Li, Y.; Luo, X.; Sun, L.; Zhao, F.; Zhang, J.; Xia, H.; Tang, Y.; Xu, S.; Wang, Y. Organic Near-Infrared Upconversion Devices: Design Principles and Operation Mechanisms. *Org. Electron.* **2016**, *31*, 258−265.

(6) Kim, D. Y.; Song, D. W.; Chopra, N.; De Somer, P.; So, F. Organic Infrared Upconversion Device. *Adv. Mater.* **2010**, *22*, 2260−2263.

(7) Yu, H.; Kim, D.; Lee, J.; Baek, S.; Lee, J.; Singh, R.; So, F. High-Gain Infrared-to-Visible Upconversion Light-Emitting Phototransistors. *Nat. Photonics* **2016**, *10*, 129−134.

(8) Baeg, K. J.; Binda, M.; Natali, D.; Caironi, M.; Noh, Y. Y. Organic Light Detectors: Photodiodes and Phototransistors. *Adv. Mater.* **2013**, *25*, 4267−4295.

(9) Dierckx, W.; Oosterbaan, W. D.; Bolsee, J. C.; Cardinaletti, I.; Maes, W.; Boyen, H. G.; D'Haen, J.; Nesladek, M.; Manca, J. Organic Phototransistors Using Poly(3-Hexylthiophene) Nanofibres. *Nanotechnology* **2015**, *26*, 065201.

(10) Luo, H.; Ban, D.; Liu, H. C.; Wasilewski, Z. R.; Buchanan, M. Optical Upconverter with Integrated Heterojunction Phototransistor and Light-Emitting Diode. *Appl. Phys. Lett.* **2006**, *88*, 073501.

(11) Chen, J.; Ban, D.; Helander, M. G.; Lu, Z.-H.; Poole, P. Near-Infrared Inorganic/Organic Optical Upconverter with an External Power Efficiency of > 100%. *Adv. Mater.* **2010**, *22*, 4900−4904.

(12) Tachibana, H.; Aizawa, N.; Hidaka, Y.; Yasuda, T. Tunable Full-Color Electroluminescence from All-Organic Optical Upconversion Devices by Near-Infrared Sensing. *ACS Photonics* **2017**, *4*, 223−227.

(13) Ullah, M.; Tandy, K.; Yambem, S. D.; Muhieddine, K.; Ong, W. J.; Shi, Z.; Burn, P. L.; Meredith, P.; Li, J.; Namdas, E. B. Efficient and Bright Polymer Light-Emitting Field Effect Transistors. *Org. Electron.* **2015**, *17*, 371−376.

(14) Zhang, C.; Chen, P.; Hu, W. Organic Light-Emitting Transistors: Materials, Device Configurations, and Operations. *Small* **2016**, *12*, 1252−1294.

(15) Muhieddine, K.; Ullah, M.; Maasoumi, F.; Burn, P. L.; Namdas, E. B. Hybrid Area-Emitting Transistors: Solution Processable and with High Aperture Ratios. *Adv. Mater.* **2015**, *27*, 6677−6682.

(16) Muccini, M. A Bright Future for Organic Field-Effect Transistors. *Nat. Mater.* **2006**, *5*, 605−613.

(17) Ullah, M.; Tandy, K.; Li, J.; Shi, Z.; Burn, P. L.; Meredith, P.; Namdas, E. B. High-Mobility, Heterostructure Light-Emitting Transistors and Complementary Inverters. *ACS Photonics* **2014**, *1*, 954−959.

(18) Song, L.; Hu, Y.; Li, D.; Chen, H.; Liu, X. Pixeled Electroluminescence from Multilayer Heterostructure Organic Light-Emitting Transistors. *J. Phys. Chem. C* **2015**, *119*, 20237−20243.

(19) Santos, L. F.; Faria, R. M.; Del Caño, T.; de Saja, J. A.; Constantino, C. J. L.; Amorim, C. A.; Mergulhão, S. Observation of

Persistent Photoconductivity in Vanadyl Phthalocyanine. *J. Phys. D: Appl. Phys.* **2008**, *41*, 125107.
(20) Ru, J.; Kojima, K.; Mizutani, T.; Ochiai, S. Deposition Process and Morphology of Metal−Phthalocyanine Thin Film Evaluated by Analyzing the Ultraviolet−Visible Spectrum and X-Ray Diffraction Profile. *Jpn. J. Appl. Phys.* **2010**, *49*, 01AE07.
(21) Wang, H.; Zhu, F.; Yang, J.; Geng, Y.; Yan, D. Weak Epitaxy Growth Affording High-Mobility Thin Films of Disk-Like Organic Semiconductors. *Adv. Mater.* **2007**, *19*, 2168−2171.
(22) Tada, H.; Saiki, K.; Koma, A. Structural Analysis of Lead Phthalocyanine Ultrathin Films Grown on Cleaved Faces of Alkali Halides by Reflection High Energy Electron Diffraction. *Surf. Sci.* **1992**, *268*, 387−396.
(23) Pan, F.; Tian, H.; Qian, X.; Huang, L.; Geng, Y.; Yan, D. High Performance Vanadyl Phthalocyanine Thin-Film Transistors Based on Fluorobenzene End-Capped Quaterthiophene as the Inducing Layer. *Org. Electron.* **2011**, *12*, 1358−1363.
(24) Kolotovska, V.; Friedrich, M.; Zahn, D. R. T.; Salvan, G. Magnetic Field Influence on the Molecular Alignment of Vanadyl Phthalocyanine Thin Films. *J. Cryst. Growth* **2006**, *291*, 166−174.
(25) Cai, X.; Zhang, Y.; Qi, D.; Jiang, J. Density Functional Theory Study on the Semiconducting Properties of Metal Phthalocyanine Compounds: Effect of Axially Coordinated Ligand. *J. Phys. Chem. A* **2009**, *113*, 2500−2506.
(26) Tao, Y.; Wang, Q.; Yang, C.; Zhong, C.; Qin, J.; Ma, D. Multifunctional Triphenylamine/Oxadiazole Hybrid as Host and Exciton-Blocking Material: High Efficiency Green Phosphorescent OLEDs Using Easily Available and Common Materials. *Adv. Funct. Mater.* **2010**, *20*, 2923−2929.
(27) Qian, C.; Sun, J.; Kong, L.; Gou, G.; Zhu, M.; Yuan, Y.; Huang, H.; Gao, Y.; Yang, J. High-Performance Organic Heterojunction Phototransistors Based on Highly Ordered Copper Phthalocyanine/Para-Sexiphenyl Thin Films. *Adv. Funct. Mater.* **2017**, *27*, 1604933.
(28) Wang, H.; Zhou, Y.; Roy, V. A. L.; Yan, D.; Zhang, J.; Lee, C. Polymorphism and Electronic Properties of Vanadyl-Phthalocyanine Films. *Org. Electron.* **2014**, *15*, 1586−1591.
(29) Li, L.; Tang, Q.; Li, H.; Hu, W. Molecular Orientation and Interface Compatibility for High Performance Organic Thin Film Transistor Based on Vanadyl Phthalocyanine. *J. Phys. Chem. B* **2008**, *112*, 10405−10410.
(30) Song, L.; Hu, Y.; Zhang, N.; Li, Y.; Lin, J.; Liu, X. Improved Performance of Organic Light-Emitting Field-Effect Transistors by Interfacial Modification of Hole-Transport Layer/Emission Layer: Incorporating Organic Heterojunctions. *ACS Appl. Mater. Interfaces* **2016**, *8*, 14063−14070.
(31) Kang, H. S.; Choi, C. S.; Choi, W. Y.; Kim, D. H.; Seo, K. S. Characterization of Phototransistor Internal Gain in Metamorphic High-Electron-Mobility Transistors. *Appl. Phys. Lett.* **2004**, *84*, 3780−3782.
(32) Xu, Y.; Berger, P. R.; Wilson, J. N.; Bunz, U. H. F. Photoresponsivity of Polymer Thin-Film Transistors Based on Polyphenyleneethynylene Derivative with Improved Hole Injection. *Appl. Phys. Lett.* **2004**, *85*, 4219−4221.
(33) Noh, Y. Y.; Kim, D. Y.; Yoshida, Y.; Yase, K.; Jung, B. J.; Lim, E.; Shim, H. K. High-Photosensitivity P-Channel Organic Phototransistors Based on a Biphenyl End-Capped Fused Bithiophene Oligomer. *Appl. Phys. Lett.* **2005**, *86*, 043501.
(34) Wang, Y.; Zhang, Y.; Lu, Y.; Xu, W.; Mu, H.; Chen, C.; Qiao, H.; Song, J.; Li, S.; Sun, B.; Cheng, Y.; Bao, Q. Hybrid Graphene-Perovskite Phototransistors with Ultrahigh Responsivity and Gain. *Adv. Opt. Mater.* **2015**, *3*, 1389−1396.
(35) Mukherjee, B.; Mukherjee, M.; Choi, Y.; Pyo, S. Organic Phototransistor with N-Type Semiconductor Channel and Polymeric Gate Dielectric. *J. Phys. Chem. C* **2009**, *113*, 18870−18873.
(36) Du, L.; Luo, X.; Zhao, F.; Lv, W.; Zhang, J.; Peng, Y.; Tang, Y.; Wang, Y. Toward Facile Broadband High Photoresponse of Fullerene Based Phototransistor from the Ultraviolet to the Near-Infrared Region. *Carbon* **2016**, *96*, 685−694.
(37) Qi, Z.; Cao, J.; Li, H.; Ding, L.; Wang, J. High-Performance Thermally Stable Organic Phototransistors Based on PSeTPTI/$PC_{61}BM$ for Visible and Ultraviolet Photodetection. *Adv. Funct. Mater.* **2015**, *25*, 3138−3146.
(38) Mukherjee, B. Large Photoresponse from a Small Molecule: Application in Photodetector and Pseudo-Transistor. *Optik* **2015**, *126*, 1258−1262.
(39) Wu, G.; Chen, C.; Liu, S.; Fan, C.; Li, H.; Chen, H. Solution-Grown Organic Single-Crystal Field-Effect Transistors with Ultrahigh Response to Visible-Blind and Deep UV Signals. *Adv. Electron. Mater.* **2015**, *1*, 1500136.
(40) Liu, S.; Su, T.; Chang, P.; Yeh, T. H.; Li, Y.; Huang, L.; Chen, Y.; Lin, C. ITO-Free, Efficient, and Inverted Phosphorescent Organic Light-Emitting Diodes Using a WO_3/Ag/WO_3 Multilayer Electrode. *Org. Electron.* **2016**, *31*, 240−246.
(41) Ikai, M.; Tokito, S.; Sakamoto, Y.; Suzuki, T.; Taga, Y. Highly Efficient Phosphorescence from Organic Light-Emitting Devices with an Exciton-Block Layer. *Appl. Phys. Lett.* **2001**, *79*, 156−158.
(42) Tandy, K.; Ullah, M.; Burn, P. L.; Meredith, P.; Namdas, E. B. Unlocking the Full Potential of Light Emitting Field-Effect Transistors by Engineering Charge Injection Layers. *Org. Electron.* **2013**, *14*, 2953−2961.
(43) Zakharko, Y.; Held, M.; Sadafi, F. Z.; Gannott, F.; Mahdavi, A.; Peschel, U.; Taylor, R. N.; Zaumseil, J. On-Demand Coupling of Electrically Generated Excitons with Surface Plasmons Via Voltage-Controlled Emission Zone Position. *ACS Photonics* **2016**, *3*, 1−7.

DOI: 10.1021/acsami.7b10538
ACS Appl. Mater. Interfaces 2017, 9, 36103−36110